# Influence of Stratigraphic Variability and Layering on Liquefiable Soils Near and Away from Structures

Lianne Brito, S.M.ASCE,<sup>1</sup> Caroline Bessette, S.M.ASCE,<sup>2</sup> Shideh Dashti, M.ASCE,<sup>3</sup> Abbie B. Liel, F.ASCE,<sup>4</sup> and Brad Wham, M. ASCE<sup>5</sup>

<sup>1</sup>Ph.D. Student, Dept. of Civil, Environmental, and Architectural Engineering, Univ. of Colorado Boulder, Boulder, CO. E-mail: <a href="mailto:lianne.brito@colorado.edu">lianne.brito@colorado.edu</a>

<sup>2</sup>Ph.D. Student, Dept. of Civil, Environmental, and Architectural Engineering, Univ. of Colorado Boulder, Boulder, CO. E-mail: <u>caroline.bessette@colorado.edu</u>

<sup>3</sup>Associate Professor, Dept. of Civil, Environmental, and Architectural Engineering, Univ. of Colorado Boulder, Boulder, CO 80309. E-mail: <a href="mailto:shideh.dashti@colorado.edu">shideh.dashti@colorado.edu</a>

<sup>4</sup>Professor, Dept. of Civil, Environmental, and Architectural Engineering, Univ. of Colorado Boulder, Boulder, CO. E-mail: abbie.liel@colorado.edu

<sup>5</sup>Assistant Research Professor, Dept. of Civil, Environmental, and Architectural Engineering, Univ. of Colorado Boulder, Boulder, CO. E-mail: <a href="mailto:brad.wham@colorado.edu">brad.wham@colorado.edu</a>

# **ABSTRACT**

Seismic soil-structure interaction (SSI), stratigraphic variability, and layering influence liquefaction triggering, the resulting total surface deformations, and damage to buildings and infrastructure. The existing empirical procedures for evaluating liquefaction triggering are primarily based on case history observations of surface manifestation and treat susceptible granular deposits as uniform and isolated. Meanwhile, most natural granular deposits are spatially variable due to heterogeneities in soil hydraulic conductivity, layer thickness, relative density, and continuity. In this paper, three-dimensional (3D), fully coupled, nonlinear finite-element analyses (FEA) in OpenSees, validated with centrifuge experimental results, are used to systematically evaluate the influence of layering and stratigraphic variations on the system's performance. We evaluate the response of two dissimilar, multi-degree-of-freedom (MDOF), shallow-founded structures. The ejecta potential index (EPI) is used to quantify the potential for formation of soil ejecta in different configurations. EPI is shown to depend strongly on the location of the groundwater table, average thickness and continuity of the liquefiable layer, and properties of and proximity to the structure. The mechanisms of deformation captured by a continuum FEA (volumetric and deviatoric) as well as the extent of softening (quantified with r<sub>u</sub>) within the critical layer are shown as uncorrelated with EPI, which depends primarily on the nature of hydraulic gradients developed within the profile. The results point to the importance of considering stratigraphic variability and potential variations in groundwater table together with average soil properties and structural characteristics when evaluating the ejecta potential on liquefiable sites.

# INTRODUCTION

Recent studies have successfully advanced our understanding of shallow-founded structures' response on liquefiable soils using shaking table physical model tests at 1g or in the centrifuge or using numerical continuum models (Bullock et al. 2019; Orang et al. 2021; Paramasivam et al. 2019). However, the main limitation of most prior studies is their inability to realistically represent variable deposits that account for heterogeneity and layering in the horizontal direction, as is often

found in the field. Previous field case histories have shown how the geometry and layering in the subsurface can affect the buildup and redistribution of excess pore pressures, shear and volumetric strains, surface ejecta manifestation, and accelerations that could impact the performance of structures or slopes (Beyzaei et al. 2018; Cubrinovski et al. 2019). Following the 2010-2011 Canterbury Earthquake Sequence in Christchurch, New Zealand, Luque and Bray (2017) studied two shallow-founded multistory buildings that suffered different levels of liquefaction-induced settlement damage. The two buildings had different degrees of stratigraphic variability and layer discontinuity underneath the structures, but both experienced sediment ejecta to some extent and permanent differential settlements. Overall, the relation between interlayering and stratigraphic variability with various mechanisms of deformation in liquefiable deposits both in the far-field and near-field is not well understood, nor are the detrimental effects on infrastructure. In this paper, the influence of layering, stratigraphic variations in one horizontal direction, and vertical changes in the groundwater table near and away from two dissimilar structures are investigated numerically through a limited sensitivity study, calibrated and validated with centrifuge tests. The results are compared in terms of different engineering demand parameters of interest, particularly the deviatoric and volumetric components of foundation deformation that are captured numerically. The potential for ejecta formation is indirectly evaluated through an index that depends on the extent of hydraulic gradients developed during dynamic loading.

# CENTRIFUGE AND NUMERICAL COMPARISONS

Centrifuge experiments at the University of Colorado Boulder's (CU's) 5.5 m-radius, 400 gton centrifuge facility assessed the seismic response of shallow-founded multiple-degree-offreedom (MDOF) structures on layered, liquefiable deposits with and without a thin lowpermeability silt cap (Paramasivam et al. 2019; Bessette et al. 2022). Two of these tests (prepared in a flexible-shear-beam, FSB container), along with their instrumentation layouts, are shown in Figure 1. These tests serve as validation models for the numerical simulations presented in this paper. The two model buildings were designed (Olarte et al. 2017) as 3- and 9-story potentially inelastic, moment-resisting steel frame structures on a mat foundation and a single-story basement (Structures A and B, respectively). Structures A and B were simplified as 3-degree-of-freedom (3-DOF) and 2-DOF models, respectively. They both represented the same foundation footprint size (9.56 m x 9.56 m in prototype scale), but the static bearing pressure of Structures A and B were 80 kPa and 187 kPa, respectively. The total thickness of both profiles was kept at 18 m. For both centrifuge experiments, the dense bottom layer consisted of a 10 m-thick layer of Ottawa F65 sand, which was dry-pluviated to achieve a relative density (D<sub>r</sub>) of about 90%. This dense layer was overlaid by a 6 m-thick loose liquefiable layer of the same material with  $D_r \approx 40\%$ . For Test  $A_{UM}$ , a 2 m-thick layer of Monterey 0/30 sand was placed at a  $D_r \approx 90\%$ , representing the non-liquefiable crust layer. For Test B<sub>UM,Silt</sub>, the top Monterey sand layer was replaced by a 0.5 m-thick layer of silica silt, Sil-Co-Sil 102 overlaid by a 1.5 m-thick layer of the Monterey sand crust. Paramasivam et al. 2019 provides properties of the soil layers used in the centrifuge models.

The two tests were spun to a centrifugal acceleration of 70 g. Each centrifuge test was subjected to a series of one-dimensional (1D) horizontal earthquake motions after saturation (with a methylcellulose solution representing a viscosity 70 times greater than water). Due to the increase in model disturbance with each motion, only the first major motion is used for the numerical validation in this paper. The acceleration response spectrum (5%-damped),  $S_a$  for this first motion recorded among different centrifuge experiments, Kobe-L, is shown in Figure 1c.

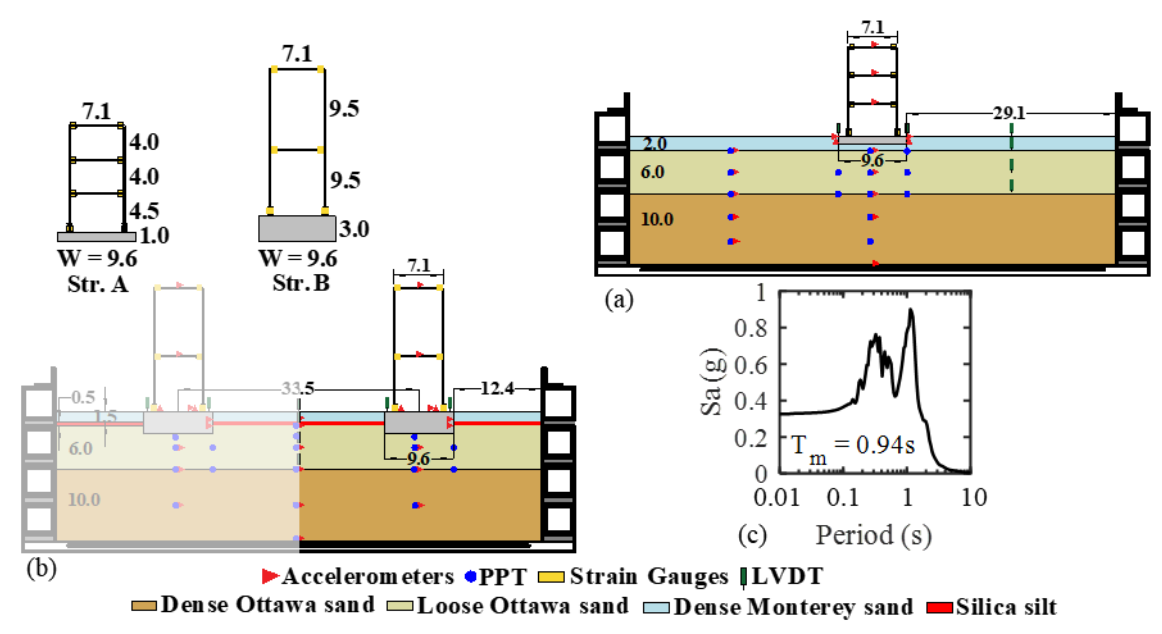


Figure 1. Instrumentation layout of the centrifuge experiments used for numerical validation in elevation view (all units are in prototype scale, meters): (a) Aum; (b) Bum.sih; (c) response spectrum (5%) of the base acceleration recorded during the first major event, Kobe-L used as input for the validation of numerical models.

The 3D, fully coupled, nonlinear, finite-element (FE) simulations were performed in the object-oriented, parallel computing, FE computational OpenSees platform (Mazzoni et al. 2006). Figure 2a shows a schematic of the numerical simulation for Model A<sub>UM</sub> as a representative case. As shown in Figure 2a, only half of the corresponding container's width was modeled for all the models due to symmetry. To mitigate boundary effects on the computed engineering parameters, the domain length (parallel to shaking) was selected as 6B (where B is the foundation width), and the domain width (perpendicular to shaking) as 3B (as determined through a sensitivity study by Hwang et al. 2022). The nodes at the lateral boundary were tied to move together in the x-direction to simulate periodic boundary conditions in the FSB box. The top nodes of the model were set as pervious to represent the water table's location. The acceleration time history for the Kobe-L input motion was applied to the soil model's bottom nodes (which were fixed in all directions).

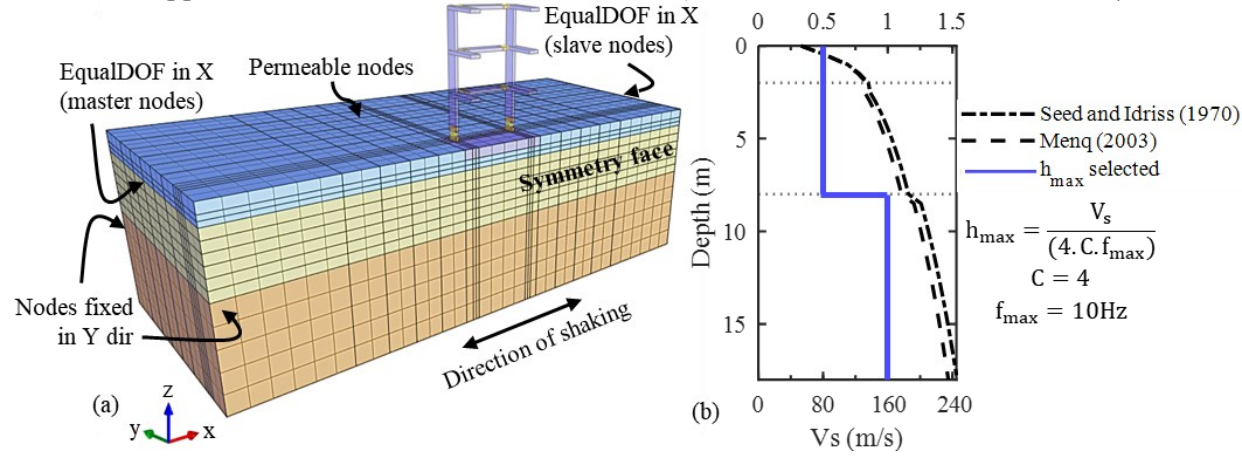


Figure 2. (a) Schematic of the numerical simulation of Model Aum as a representative case, with the assigned boundary conditions; and (b) V<sub>s</sub> profile and selection of element size.

The nonlinear response of soil was simulated with the pressure-dependent, multi-yield surface, version 2, soil constitutive model (Elgamal et al. 2002; Yang et al. 2008), PDMY02, with soil model parameters adopted from Hwang et al. (2022). The calibration process was based on monotonic and cyclic, drained and undrained triaxial tests (Badanagki 2019), a free-field centrifuge experiment with the same soil types (Ramirez et al. 2018), and field observations in terms of cyclic stress ratio (CSR) to trigger liquefaction in 15 cycles (NCEER 1997). The soil elements were modeled as solid-fluid, 20-8 node BrickUP elements. The maximum allowable element height was determined at each depth based on the small-strain shear wave velocity,  $V_s$  (Seed and Idriss 1970; Menq 2003) of the soil profile, in addition to the maximum frequency of the input motion in the centrifuge (e.g.,  $f_{max} = 10$  Hz in prototype scale). The final selection of element size and  $V_s$  is shown in Figure 2b.

Elastic (steel) beam-column elements represent the beams and columns in the superstructure. Nonlinear beam-column elements were used to model the fuse components, which were discretized into fiber sections. The stress-strain behavior of the fibers were represented by a uniaxial steel material (Giuffre and Pinto 1970). Inertial masses and gravity loads were added to each floor level of the superstructure. Structure nodes only allow in-plane translational deformations and rotations at the symmetry face. The mat foundation and single-story basement were modeled using 20-8 BrickUP elements and were assigned a linear elastic material. To prevent excess pore pressure generation, the fluid mass density was set to zero. An equal DOF interaction allowed the foundation elements to connect to the surrounding soil. At the foundation's lateral perimeter, the nodes were linked to the soil in the x- and y-directions to allow for relative settlement, while the bottom foundation nodes were connected to the soil in all three directions.

Figure 3 compares experimental and numerical results in terms of S<sub>a</sub> and settlement time histories of foundations, excess pore water pressure (EPWP) time histories, and S<sub>a</sub> under the center of the structure in the middle of the liquefiable layer. The results show that numerical simulations could roughly capture the general trends for both structures observed experimentally in terms of foundation's permanent settlement (difference of less than 5% in each response).

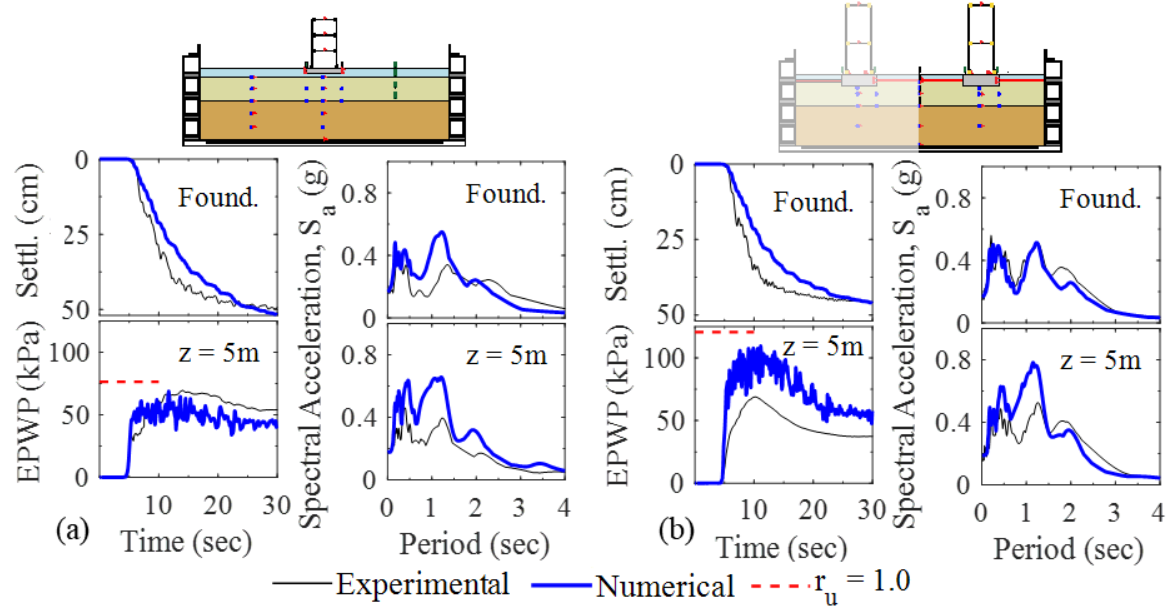


Figure 3. Comparison of experimental and numerical results in terms of 5%-damped Sa and settlements of foundations, excess pore pressure time histories, and Sa under the center of Structures: (a) Aum; (b) Bum.silt in the middle of the critical layer during Kobe-L.

As shown in Figure 3, the peak EPWP was overestimated for Model  $B_{UM,Silt}$  by about 45%. We attribute this discrepancy to potential fractures within the silt layer in the experiment that led to higher EPWP dissipation due to foundation B's greater embedment, interrupting the silt layer continuity. For Model  $A_{UM}$  the numerical simulation overestimated the foundation  $S_a$  near the structure's fundamental period ( $T_{o\text{-}A} \approx 0.57~\text{sec}$ ) by about 63%. This discrepancy could be partly due to the numerical overestimation of the dilation cycles, leading to acceleration spikes at lower periods. In summary, factoring in possible sources of error and uncertainty in both numerical and experimental results, we deemed the comparison presented in Figure 3 to be reasonable for the next step of evaluating the effects of stratigraphic variability on system performance.

# IMPACT OF STRATIGRAPHIC VARIABILITY AND LAYERING ON SYSTEM PERFORMANCE

# Design of the numerical sensitivity study

As part of a limited sensitivity study, 24 3D simulations were performed to evaluate the influence of stratigraphic variability and layering on system performance. These 24 simulations vary the location of the groundwater table, the number of critical, loose, and saturated Ottawa layers, the number of low permeability silt layers distributed within the profile, and the liquefiable layer thickness variability (slope) in the horizontal direction (Figure 4). These parameters were informed by a combination of observed trends in the Hutabarat (2020) case history database of near-building site conditions with ejecta severity ranging from none to extreme and Zupan (2014) case history database of buildings with sloped critical layers. The goal of the small sensitivity study was to introduce a level of complexity with each profile configuration by starting with ID 1 as the typical uniform layered profile studied in the past (and validated with centrifuge) and from there, maintaining the same average thickness for the critical liquefiable layer (6 m) but introducing silt interlayers of 0.5 m thickness (ID 2 and ID 3). In ID 4, we introduce multiple liquefiable layers that add to the same cumulative liquefiable layer thickness as the previous profiles (6 m), and then for ID 5, we introduce silt caps at the boundaries of each liquefiable layer. Lastly, ID 6 represents a non-uniform sloped critical layer in the horizontal direction. The limited sensitivity study aims to systematically evaluate how the progression of these realistic soil profile variations influence the system's performance. To accomplish this goal, we only varied the location of the groundwater table (location at the surface and at 2 m depth) and the type of structure studied (Structure A and B) for each of the 6 profiles, while keeping other parameters constant, such as the input ground motion and all other soil properties. In summary, we conducted four analyses for each of the 6 profiles shown in Figure 4, alternating the structure type (A and B) and groundwater table location (0 and 2 m named as wt0m and wt2m), adding to 24 3D SSI simulations.

The outcropping rock earthquake motion was selected from the shallow crustal earthquake database by Bullock et al. (2017). The two horizontal recordings were rotated to find maximum rotated (RotD100) peak ground acceleration. The ground motions were baseline-corrected and filtered (using a band-pass filter with corner frequencies of 0.1 and 12 Hz). To pick the input motion for the numerical models, the ground motions in the database were divided into intensity levels according to the cumulative absolute velocity (CAV) of outcropping ground motions. We use CAV for this purpose because CAV has previously been shown to correlate better with settlement predictions (Karimi et al. 2018 and Bullock et al. 2019a). We focused on motions in the top quantile with CAV greater than 600 cm/s, while also considering the duration of the motions

to reduce computational cost. From there, these motions were used to perform a preliminary sensitivity study on ID 1 and 5 profiles, which were expected to provide a wide range of settlement predictions. We aimed for ground motions that would cause a minimum of 2.5-3 cm (typically considered acceptable in design). The ground motion selected was the 2010 Christchurch earthquake recorded at the PARS station, with a moment magnitude ( $M_w$ ) of 6 and a rupture distance ( $R_{rup}$ ) of 3.63 km. The bedrock in the limited sensitivity study was modeled as a rigid half-space by fixing the bottom nodes in all directions. In order to convert the chosen outcrop motion to within-rock for the soil profiles, a 1D, equivalent-linear, site response analysis routine was set up in DeepSoil 7.0 (Hashash et al. 2020). The within-rock motions for each of the profiles were used as input to the numerical models with a rigid rock. The mean properties of within motions across all ID models for the selected ground motion included: (i) peak ground acceleration (PGA) = 0.51 g, (ii) significant duration  $D_{5-95}$  = 3.44 s, (iii) Arias Intensity ( $I_a$ ) = 2.2 m/s, (iv) cumulative absolute velocity ( $I_a$ ) = 749 cm/s, and (v) mean period  $I_a$  = 0.86 s.

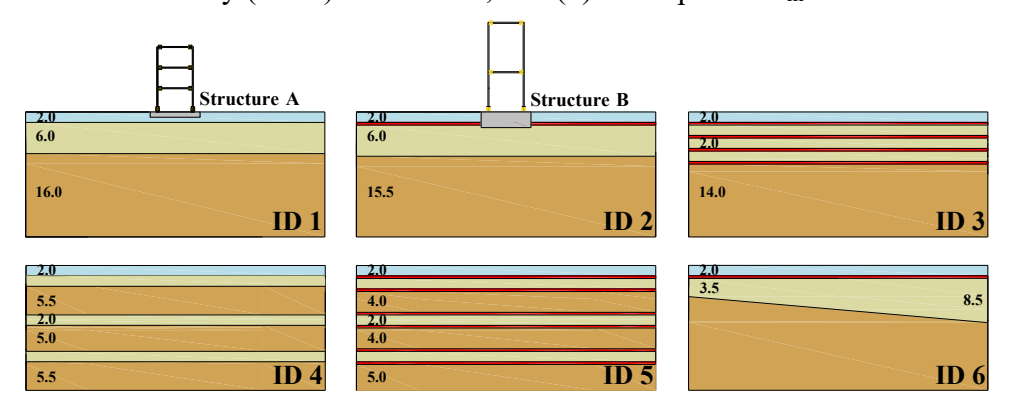


Figure 4. Schematic of representative sensitivity study profiles with Structure A and B shown in ID 1 and ID 2, respectively (units in meters).

# Response of soil and foundation

Figure 5a shows the numerically computed foundation permanent settlement and residual tilt for each of the model IDs. The influence of groundwater table variations on foundation settlement was minimum for most profiles, except for ID 1 (51% difference for Structure A and 20% for Structure B). In ID 1 for Structure A, the higher groundwater table led to increased settlement due to a reduction in effective stresses and soil stiffness under the foundation, when compared to ID 2 where the groundwater table change did not have an impact due to the silt cap, which slowed down drainage and partially mitigated settlement changes. For this specific input motion, the residual tilt became more significant for the non-uniform ID 6 profile. The authors investigated if the direction of the nonuniformity in thickness of the critical layer in relation to the ground motion would influence the tilt response by changing the polarity of the motion. The results show that for Structure B with both groundwater table configurations, the residual tilt could change by a factor of 4 depending on the direction of shaking (and its polarity) with respect to the direction of slope in the critical layer. This pattern was not substantial for the shorter and lighter Structure A.

The peak excess pore water ratio (peak  $r_u = max \; EPWP/\sigma_{zo}$ ) in the middle of the liquefiable layer at the edge and center for all analyses is presented in Figure 5b. We stayed consistent with the objective of capturing the response at the middle of the total thickness of the loose Ottawa layer/s (e.g., z = 5 m and z = 10.5 m for IDs 1 and 5, respectively). In most configurations below

the center of the two structures, liquefaction (defined as  $r_u = 1$ ) was triggered, except in cases with multiple silt interlayers within the single liquefiable critical layer.

The influence of soil ejecta was investigated using the procedure proposed by Hutabarat (2020). In this approach, the excess pressure head required ( $h_{\rm exc} = u_{\rm e}/\gamma_{\rm w}$ ) to produce surface ejecta manifestation is equivalent to the excess head that exceeds the artesian excess head ( $h_{\rm A}$ ), represented as a 1:1 sloped line across the depth of the profile limited to the maximum excess head ( $\max h_{\rm exc} = \sigma_{\rm zo'}/\gamma_{\rm w}$ ). The ejecta potential index (EPI), shown in Figure 5c and d for our profile configurations, is bounded by the duration of artesian conditions (a minimum time when input acceleration reaches 0.05 g and a maximum of 150 s) and the upper 10 m of the profile, which is assumed to provide most of the demand. Figure 5c presents the EPI results under the center and edge of the structures. Given the complexity and computational time of the 3D models, we only performed each analysis for the maximum duration of the motion (20 s), hence the EPI<sub>20</sub> naming used in Figure 5c, meaning that it was calculated at 20 s instead of the recommended 150 s by Hutabarat (2020). The ejecta manifestation severity is categorized as minor (10 - 40 m<sup>3</sup>·s), moderate (40 - 100 m<sup>3</sup>·s), severe (100 - 300 m<sup>3</sup>·s), and extreme (greater than 300 m<sup>3</sup>·s).

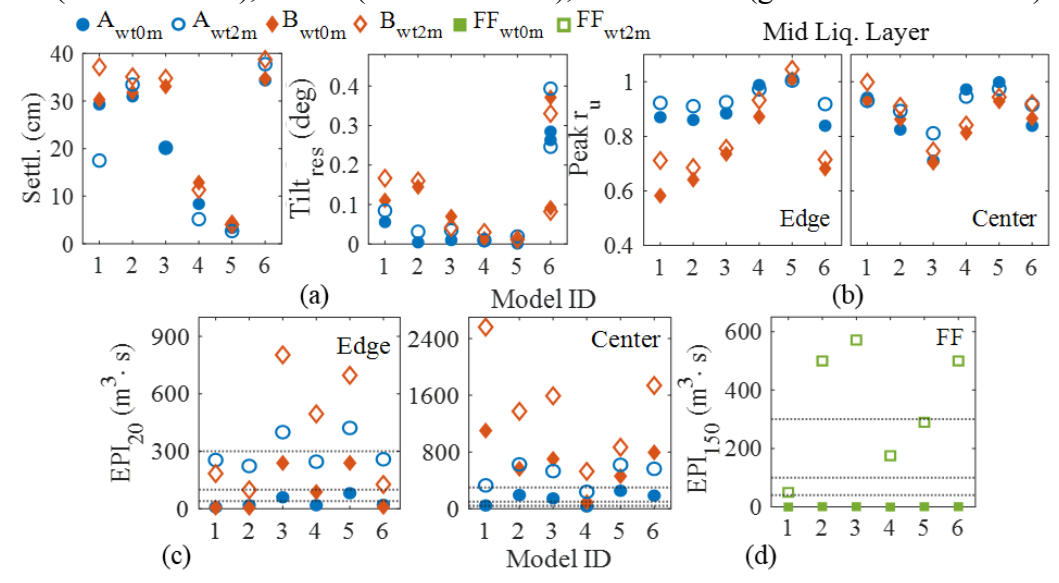


Figure 5. (a) Foundation permanent settlement and tilt; (b) peak r<sub>u</sub> at the middle of the liquefiable layer at the edge and center of Structures A and B; (c) EPI for 20 s duration motion at the edge and center of Structures A and B; and (d) EPI for 150 s duration motion representing the free-field response. The dashed black lines represent the ejecta manifestation severity category from minor to extreme.

For near-field conditions, at the foundation's edge, only cases with the lower groundwater table are categorized as extreme ejecta manifestation. For Structure A models with the groundwater table at the surface, in both the center and edge of the foundation, all were classified as severe or lower. Below the foundation's center, the combination of Structure's B higher embedment and bearing pressure, along with the lower groundwater table, led to an extreme classification in all cases. Figure 5d shows the EPI for free-field conditions evaluated through single soil column analyses representing the same soil profile configurations. For this case, computational time was not a constraint, and the analyses were conducted for 150 s, representing the EPI<sub>150</sub> results. Free-field soil profiles with a surface groundwater table predicted no ejecta manifestation, according to the EPI classification. Profiles with the groundwater table at 2 m and one or multiple silt layers

within the liquefiable layer estimated extreme liquefaction surficial manifestation. The presence of silt interlayers was not necessary to drive EPI in the moderate or higher category; however, all the cases with silt interlayers resulted in EPI values greater than those without silt interlayers.

Figure 6 highlights the numerical residuals for different engineering demand parameters of interest with respect to the baseline case (soil ID 1 with Structure A and groundwater table at the surface). The calculation of the logarithmic residual, r, is based on Equation 1:

$$r = \ln(\text{Model ID}) - \ln(\text{ID1}_{\text{Str A wt0m}}) \tag{1}$$

where ln(Model ID) and ln(ID1<sub>Str A wt0m</sub>) are the natural logarithms of each model ID and baseline case, respectively. Hence, the baseline case represents a zero residual, and a positive and negative residual value represents a result greater and lower than the baseline case, respectively. The settlement results only show deviation for the profiles with multiple liquefiable layers (ID 4 and 5), which was expected due to the reduction in thickness of the shallower liquefiable layer which affects volumetric settlement. For these cases, there is also a reduction in softening due to the smaller excess pore pressures generated in a smaller volume of loose sand, which would lead to a decrease in predicted settlements, as observed. The lower groundwater table consistently resulted in higher EPI values, likely due to faster dissipation, preventing artesian flow initiation. Upon evaluating the square of the correlation coefficient (R<sup>2</sup>) for combinations of settlement, peak r<sub>u</sub> and EPI under the center and edge of the structure, the maximum R<sup>2</sup> value was calculated as 0.24. Therefore, our results show no correlation between the mechanisms of displacement captured by the FE continuum framework (volumetric strains due to consolidation and partial drainage as well as deviatoric) and the magnitude of ejecta quantified indirectly by the EPI, since these are different mechanisms of deformation. Overall, the effect of stratigraphic variability and interlayering does not impact the majority of the engineering demand parameters predicted by continuum FEAs. The residual results inform us that only the ejecta proxy, evaluated through EPI, varied the most depending on the location of the groundwater table, average thickness and continuity of the liquefiable layer, and properties of and proximity to the structure. Additional simulations with a range of structural and ground motion parameters are needed to identify key EPI predictors.

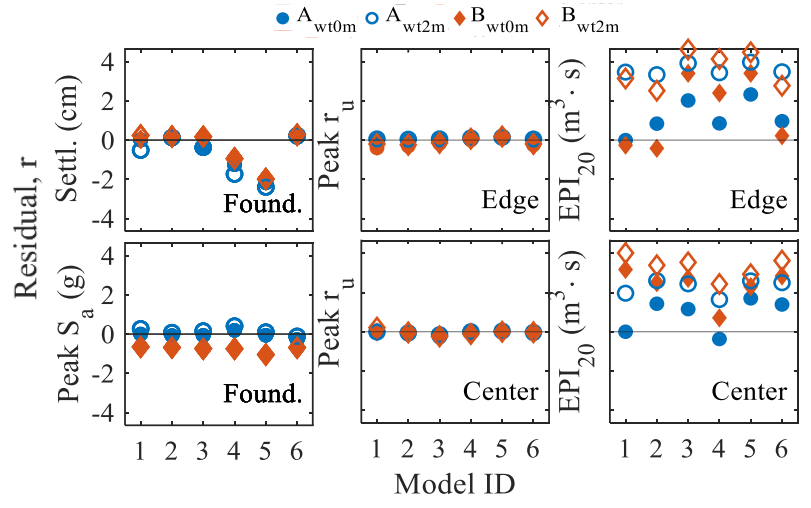


Figure 6. Numerical residuals for different engineering demand parameters (EDPs) with respect to soil profile ID 1 with Structure A and groundwater table at the surface, assigned as the baseline case and represented with the solid black line.

#### SUMMARY AND CONCLUSIONS

This study provides insights into the influence of stratigraphic variability and layering on liquefiable soils near and away from structures. We present the results of two centrifuge experiments that evaluate the response of two isolated different structures on layered, liquefiable soil profiles with and without a thin low-permeability silt cap. These experimental results served to validate the fully coupled, nonlinear, effective-stress numerical simulations. A limited numerical sensitivity study followed to evaluate the impact of the geometry and layering of the profile, location of the groundwater table, and building properties on the seismic response at a systems level. The results for different engineering demand parameters of interest are presented for all the simulations, as well as the numerical residuals based on a baseline case to determine deviation influences. The simulations show that 3D continuum numerical models do not capture the effects of subtle variations in the profile or groundwater table location for the majority of engineering demand parameters. The effect of stratigraphic variability and layering is most eminent in the potential for the formation of soil ejecta, quantified through EPI. This small sensitivity study sets the stage for a numerical database that considers realistically variable deposits to facilitate future predictive models of building performance.

#### **ACKNOWLEDGEMENTS**

Funding from the Graduate Assistance in Areas of National Need (GAANN), and the NSF Graduate Research Fellowship (GRFP) is gratefully acknowledged. This work utilized the Alpine high-performance computing resource at CU Boulder. Alpine is jointly funded by CU Boulder, CU Anschutz, Colorado State University, and the National Science Foundation (award 2201538).

# REFERENCES

- Badanagki, M. (2019). "Influence of dense granular columns on the seismic performance of level and gently sloped liquefiable sites." Ph.D. thesis. Univ. of Colorado Boulder.
- Bessette, C., Hwang, Y. W., Brito, L., Dashti, S., Wham, B., Liel, A., & Westcott, J. (2022). "Influence of Domain Boundaries on the Response of Isolated Structures on Liquefiable Soils." In *Geo-Congress* 2022 (pp. 297-307).
- Beyzaei, C. Z., Bray, J. D., van Ballegooy, S., Cubrinovski, M., & Bastin, S. (2018). "Depositional environment effects on observed liquefaction performance in silt swamps during the Canterbury earthquake sequence." *Soil Dyn. Earthq. Eng.*, 107, 303-321.
- Bullock, Z., Dashti, S., Liel, A., Porter, K., Karimi, Z., & Bradley, B. (2017). "Ground-motion prediction equations for Arias intensity, cumulative absolute velocity, and peak incremental ground velocity for rock sites in different tectonic environments." *Bulletin of the Seismological Society of America*, 107(5), 2293-2309.
- Bullock, Z., Karimi, Z., Dashti, S., Porter, K., Liel, A. B., & Franke, K. W. (2019a). "A physics-informed semi-empirical probabilistic model for the settlement of shallow-founded structures on liquefiable ground." *Géotechnique*, 69(5), 406-419.
- Cubrinovski, M., Rhodes, A., Ntritsos, N., & Van Ballegooy, S. (2019). "System response of liquefiable deposits." *Soil Dyn. Earthg. Eng.*, 124, 212-229.
- Elgamal, A., Yang, Z., & Parra, E. (2002). "Computational modeling of cyclic mobility and post-liquefaction site response." *Soil Dyn. Earthq. Eng.*, 22(4), 259-271.

- Giuffrè, A., and P. E. Pinto. (1970). "Il comportamento del cemento armato per sollecitazioni cicliche di forte intensità." *Giornale del Genio Civile, Maggio, 5* (1): 391–408.
- Hashash, Y.M.A., Musgrove, M.I., Harmon, J.A., Ilhan, O., Xing, G., Numanoglu, O., Groholski, D.R., Phillips, C.A., and Park, D. (2020). "DEEPSOIL 7, User Manual". Urbana, IL, Board of Trustees of University of Illinois at Urbana-Champaign.
- Hutabarat, D. (2020). "Effective stress analysis of liquefaction sites and evaluation of sediment ejecta potential." Ph.D. thesis. Univ. of California, Berkeley.
- Hwang, Y. W., Bullock, Z., Dashti, S., & Liel, A. (2022). "A Probabilistic Predictive Model for Foundation Settlement on Liquefiable Soils Improved with Ground Densification." *J. Geotech. Geoenviron. Eng.*, 148(5), 04022017.
- Jahed Orang, M., Motamed, R., Prabhakaran, A., & Elgamal, A. (2021). "Large-scale shake table tests on a shallow foundation in liquefiable soils." *J. Geotech. Geoenviron. Eng.*, 147(1), 04020152.
- Karimi, Z., Dashti, S., Bullock, Z., Porter, K., & Liel, A. (2018). "Key predictors of structure settlement on liquefiable ground: a numerical parametric study." *Soil Dyn. Earthq. Eng.*, 113, 286-308.
- Luque, R., & Bray, J. D. (2017). "Dynamic analyses of two buildings founded on liquefiable soils during the Canterbury earthquake sequence." *J. Geotech. Geoenviron. Eng.*, 143(9), 04017067.
- Mazzoni, S., McKenna, F., Scott, M. H., & Fenves, G. L. (2006). Open system for earthquake engineering simulation user command-language manual. *Pacific Earthquake Engineering Research Center, University of California, Berkeley, OpenSees version, 1*(3).
- Menq, F. Y. (2003). "Dynamic properties of sandy and gravelly soils." Ph.D. Thesis. Univ. of Texas at Austin.
- NCEER (National Center for Earthquake Engineering Research). 1997. Proceedings of the NCEER workshop on evaluation of liquefaction resistance of soils. Technical Rep. No. NCEER-97-0022. Taipei, Taiwan: NCEER.
- Olarte, J., Paramasivam, B., Dashti, S., Liel, A., & Zannin, J. (2017). "Centrifuge modeling of mitigation-soil-foundation-structure interaction on liquefiable ground." *Soil Dyn. Earthq. Eng.*, 97, 304-323.
- Paramasivam, B., Dashti, S., & Liel, A. (2019). "Impact of spatial variations in permeability of liquefiable deposits on seismic performance of structures and effectiveness of drains." *J. Geotech. Geoenviron. Eng.*, 145(8), 04019030.
- Ramirez, J., Barrero, A. R., Chen, L., Dashti, S., Ghofrani, A., Taiebat, M., & Arduino, P. (2018). "Site response in a layered liquefiable deposit: evaluation of different numerical tools and methodologies with centrifuge experimental results." *J. Geotech. Geoenviron. Eng.*, 144(10), 04018073.
- Seed, H. B., & I. M. Idriss. (1970). "Soil moduli and damping factors for dynamic response analyses." Technical Rep. No. EERRC-70-10. Berkeley, CA: Univ. of California.
- Yang, Z., Lu, J., & Elgamal, A. (2008). OpenSees soil models and solid-fluid fully coupled elements. *User's Manual. Ver*, 1, 27.
- Zupan, J. D. (2014). "Seismic performance of buildings subjected to soil liquefaction." Ph.D. Thesis Univ. of California, Berkeley.